A Unified Perspective of RTN and BTI

T. Grasser, K. Rott•, H. Reisinger•, M. Waltl*, J. Franco°, and B. Kaczer°*

*Institute for Microelectronics, TU Wien, Austria •Infineon, Munich, Germany °imec, Leuven, Belgium

***Abstract*—It has recently been suggested that random telegraph noise (RTN) and the bias temperature instability (BTI) are due to similar defects. Here we thoroughly analyze this hypothesis using nano-scale devices to show that *(i)* all defects that contribute to BTI recovery can also become spontaneously charged to produce an RTN event, *(ii)* most RTN defects also contribute to BTI recovery, *(iii)* the distribution of step-heights, capture and emission times is equally wide and similar for RTN and BTI, and *(iv)* both RTN and BTI defects are volatile, meaning that they can disappear and reappear. From these observations we conclude that RTN and the recoverable component of BTI are very likely *due to the same defects*. As a very important consequence, RTN and BTI *must be analyzed and guardbanded against together*. In particular, since conventional RTN analysis dominantly captures defects with the strongest contribution to the noise power, it misses the defects with large capture times. As we will show, however, it is exactly these defects with large capture times that may by chance become occupied at the same time after long times, thereby leading to very large NBTI-like threshold voltage fluctuations in an RTN setting. Conversely, conventional BTI analysis based on the expectation value of the stochastic trap behavior misses these RTN-like fluctuations when extrapolated down to operating voltages, potentially leading to wrong conclusions.**

I. INTRODUCTION

Charge trapping in border traps is conventionally considered the source of RTN [1–4]. Similar traps have been associated with at least part if not all of the recoverable component of BTI, particularly for NBTI in SiON devices [5–9] and PBTI in high-k oxides [10–14]. As an alternative explanation it has been suggested that also interface states (or whatever defects are visible in charge-pumping currents [15]) can contribute to BTI recovery [15–17]. We have recently demonstrated [18] that in our technology ($W \times L = 150\,\text{nm} \times 100\,\text{nm}$, $t_{\text{ox}} = 2.2\,\text{nm}$ SiON) *all* discrete recovery events in the stress and recovery time ($100\,\mu\text{s}$ – $1\,\text{ks}$) and temperature window ($100\,^\circ\text{C}$ – $200\,^\circ\text{C}$) are due to first order processes and therefore reaction- rather than diffusion-limited. As such, being a reaction-limited process, recovery is dominantly due to detrapping from border traps, even after long stress times, suggesting a strong link between RTN and BTI defects [19]. Furthermore, it has been demonstrated that many of these defects are volatile, meaning that they can disappear and reappear on a wide range of timescales (shortest was 1 hour, longest observed was several months) [18].

In the following we will provide an in-depth analysis of the hypothesis that RTN and the recoverable component of BTI are due to the same defects. For this, we proceed as follows:

(i) On a selected nano-scale device we analyze recovery following NBTI stress using time-dependent defect spectroscopy (TDDS) and try to identify as many defects a possible.

(ii) On the same device, we perform a detailed RTN analysis using different sampling rates and sample times at different gate voltages, trying to identify contributions from the previously characterized NBTI defects by matching characteristic times and step-heights. We also search for contributions of other defects not previously identified in the NBTI experiments.

(iii) In order to check the statistical relevance of these findings, we repeat this study in a less time-consuming and therefore cruder semi-automatic manner on 100 different devices using a 1 ks initial RTN phase, followed by a BTI stress phase and a subsequent 1 ks recovery phase.

(iv) We then match initial RTN defects to steps observed in BTI recovery as well as the modification of the RTN by the stress. Furthermore, we analyze how BTI creates new RTN and also how RTN disappears, possibly as a consequence of stress.

(v) As our experiments clearly indicate that RTN and BTI are due to the same defects, we analyze the consequences of this observation.

II. EXPERIMENTAL METHOD

For the first part of our study we use a selected nano-scale device (device B from our previous study [20]) and analyze the defects contributing to NBTI recovery using the time dependent defect spectroscopy (TDDS). Given the small gate area ($W \times L = 150\,\text{nm} \times 100\,\text{nm}$), only a handful of defects are active in the measured recovery window for a certain gate bias and temperature, leading to a discrete recovery behavior. Three selected recovery traces after a 10 s long stress are shown in Fig. 1, where each discrete step is due to the emission of a single hole from the oxide. Repetition of this experiment allows for a statistical analysis of the data in the spectral maps, see Fig. 2, through identification of defects by their fingerprints: their step-height d (the defect-induced ΔV_{th}) and the emission and capture times, τ_{e} and τ_{c}.

In this particular case, the bias and temperature dependence of the capture and emission times as well as d for about seven defects are extracted. All three parameters are found to be very sensitive to the gate bias [21–23]. Typically, for defects accessible by TDDS, and therefore those contributing to BTI, τ_{c} decreases with increasing $|V_{\text{G}}|$. Above a gate bias where τ_{c} becomes smaller than τ_{e}, the defect will be predominantly charged when the stress time exceeds τ_{c}. Still, even at lower $|V_{\text{G}}|$ *any* defect can spontaneously capture a charge, although this becomes increasingly unlikely with increasing τ_{c}. Also, as at lower $|V_{\text{G}}|$ the emission times are typically much shorter than τ_{c}, this will result in occasional transient spikes of height d rather than the more obvious up-and-down jumps usually

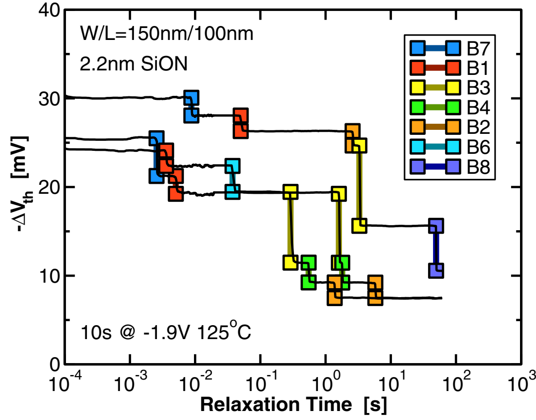

Fig. 1. The seven dominant defects of device B [20] identified by TDDS [20]. The figure shows three selected recovery traces. Defect B5 was extremely volatile and not active during this particular experiment.

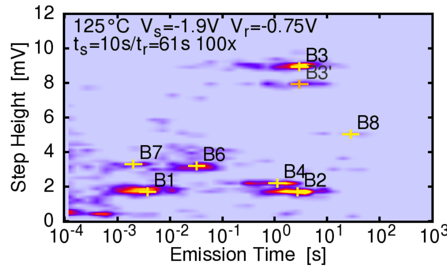

Fig. 2. The TDDS spectral map shows seven exponentially distributed clusters corresponding to the seven defects. Defect B5 was inactive, while B7 and B8 have a capture time larger 10 s and are thus only barely visible given the maximum recovery time of 61 s. The step-height of B3 depends strongly on the occupancy of other defects (range: $5-9\,\mathrm{mV}$) [21].

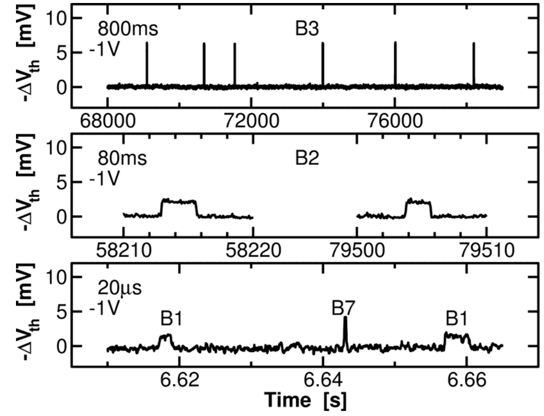

Fig. 3. By using different sampling rates it can be shown that all defects identified during NBTI recovery (cf. Fig. 1 and Fig. 2) also produce RTN. At low $|V_\mathrm{G}|$, only one defect is typically occupied at a time.

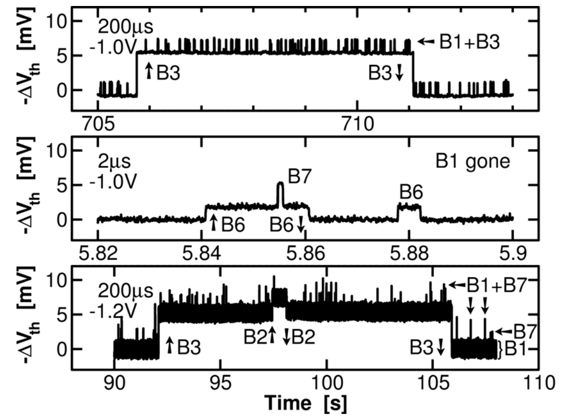

Fig. 4. By chance, individual traps can become simultaneously occupied. **Bottom**: With increasing gate bias, the probability for simultaneously occupied traps increases (shown is $V_\mathrm{G}=-1.2\,\mathrm{V}$).

associated with RTN. Using the extracted bias dependencies of the defect parameters, dedicated RTN experiments with tailored sampling rates and sampling times are run to identify as many traps contributing to RTN as possible.

We focus our search on gate biases around $V_\mathrm{DD}=-1.3\,\mathrm{V}$ in the range $-0.7\,\mathrm{V}$ to $-1.5\,\mathrm{V}$. One serious issue with RTN analysis is that several capture and emission events need to be recorded (ideally more than 100) using a sampling rate at least 100 higher than the inverse of the fastest time constant [24, 25]. For example, from TDDS analysis defect B3 is expected to have $\tau_\mathrm{c}\approx 10\,\mathrm{ks}$ and $\tau_\mathrm{e}\approx 10\,\mathrm{s}$ at $V_\mathrm{G}=-1\,\mathrm{V}$ and 125°C. By contrast, at the same conditions defect B1 is expected to be considerably faster, with $\tau_\mathrm{c}=100\,\mathrm{ms}$ and $\tau_\mathrm{e}=10\,\mathrm{ms}$. Thus in order to properly resolve both defects in a single experiment, in the ideal case 10^{10} samples would have to be taken at this bias and temperature, making both data storage as well as analysis a nuisance. We therefore adapt both sampling time and rate to the individual defects (or a suitable group of defects). Given practical constraints of our equipment, we using sampling rates in the range $1/2\,\mu\mathrm{s}$ – $1/800\,\mathrm{ms}$ and recording times in the range 4 s – 100 ks. We directly measure $\Delta V_\mathrm{th}(t)$ using our ultra-fast NBTI characterization setup [26]. The defects appearing in these $\Delta V_\mathrm{th}(t)$ traces are characterized and compared to the defects seen in the NBTI recovery traces using available $\tau_\mathrm{c}(V_\mathrm{G})$, $\tau_\mathrm{e}(V_\mathrm{G})$, and $d(V_\mathrm{G})$ data.

As can be seen for a few examples in Fig. 3, all NBTI recovery defects from Fig. 1 and Fig. 2 can be identified in the RTN traces by matching d, τ_c and τ_e. However, many of these defects have very large capture times, produce only occasional RTN events (the aforementioned spikes), and are thus typically not considered in conventional RTN analysis. An important observation is, however, that by chance individual defects can become occupied at the same time, see Fig. 4, *leading to considerably larger total RTN amplitudes* than could be expected from conventional RTN analysis of the dominant traps. The probability for this to occur increases with increasing $|V_\mathrm{G}|$.

From the RTN data, τ_c, τ_e, and d can be extracted for the BTI defects at lower $|V_\mathrm{G}|$. In this regime the TDDS often becomes impractical due to additional complications in the data analysis induced by the occurrence of RTN [27]. Also, we typically select devices for TDDS which do not produce significant RTN at the most important readout voltages (e.g. around V_th), as their the TDDS works best. The readout voltages have to be not too low in order to still generate sufficient drain current for the measurement equipment and not too high because at higher $|V_\mathrm{G}|$ the impact of a single charge on

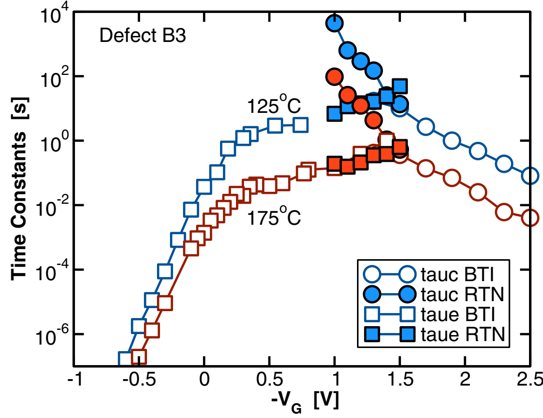

Fig. 5. The bias and temperature dependent capture and emission times determined by TDDS (open symbols) and RTN analysis (filled symbols) agree very well. The example shows defect B3.

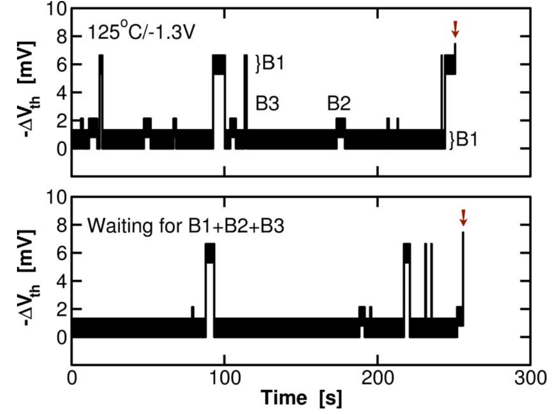

Fig. 7. The time until by chance all defects become charged is calculated using a kinetic MC method [29]. Two realizations of the stochastic process are shown above using a subset of defects (B1, B2, and B3).

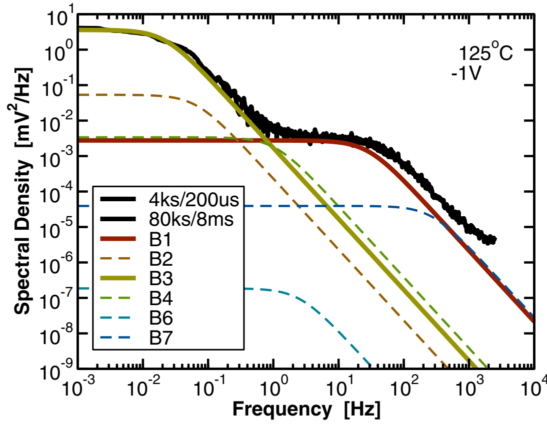

Fig. 6. The experimental power spectral density (black lines) is dominated by the defects B1 and B3. Other contributions to the PSD are negligible in the frequency range 1 mHz - 1 kHz.

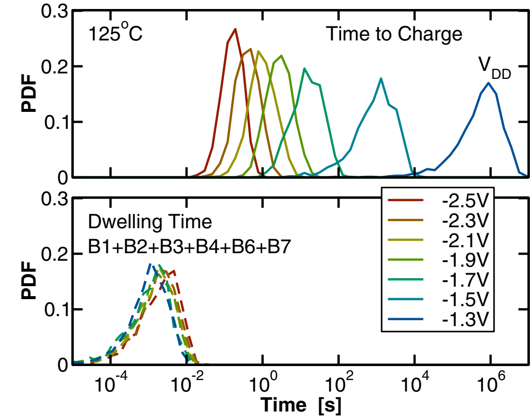

Fig. 8. **Top**: The p.d.f. of the time to charge for all defects. **Bottom**: The average dwelling time in this combined state is dominated by the defects with the shortest emission time (B1 and B7).

I_D is considerably reduced [20, 22, 23, 28]. However, due to the bias dependence of τ_c and τ_e, every defect identified in the BTI recovery trace is expected to produce RTN when a gate voltage is applied at which $\tau_c(V_G)$ is of the same order of magnitude as $\tau_e(V_G)$. The capture and emission times extracted from the RTN data should therefore complement the TDDS data at low bias conditions. That this is really the case is demonstrated in Fig. 5, where τ_c and τ_e of defect B3 are shown. *Note that the results obtained from RTN and TDDS agree perfectly*. Also noteworthy is the very large capture time of $\tau_c(-1\,V) \approx 9\,ks$.

Except for the BTI defects, no other RTN-only defects could be identified in this sample. However, to make sure no 'cherry-picking' occurred during RTN analysis, the measured power spectral density (PSD) is compared with that resulting from the theoretical value predicted by our defect analysis. For this, the extracted d_i, $\tau_{c,i}$, and $\tau_{e,i}$ of the individual defects are used to calculate a PSD as

$$S(f) = \sum \frac{(2 d_i \tau_i)^2}{(\tau_{c,i} + \tau_{e,i})(1 + (2\pi f \tau_i)^2)} \tag{1}$$

with $1/\tau_i = 1/\tau_{c,i} + 1/\tau_{e,i}$. In order to guarantee comparable conditions, the experimental reference is not obtained from a spectrum analyzer but by an FFT of the time-domain data using Welch's method for the various combinations of sampling times and rates. As shown in Fig. 6, the PSD obtained from the RTN analysis is dominated by defects B1 and B3 obtained from BTI recovery and agrees very well with the experimental observation.

III. Discussion

The above analysis has demonstrated that the defects visible during NBTI recovery also dominate the RTN signal in this sample. In particular, depending on the sampling rate, RTN will be either dominated by B1 or B3, which would be then subjected to conventional RTN analysis. The fact that it is the same defects that are responsible for RTN and the recoverable component of BTI has some important consequences, as will be discussed below.

A. Simultaneously Occupied RTN Defects

One important consequence of the above observation is that by chance multiple defects can become occupied at the same time. While it is unlikely for defects with large τ_c to contribute to this combined state, the occurrence of this is merely a matter of time. As such, even though such cases will rarely occur

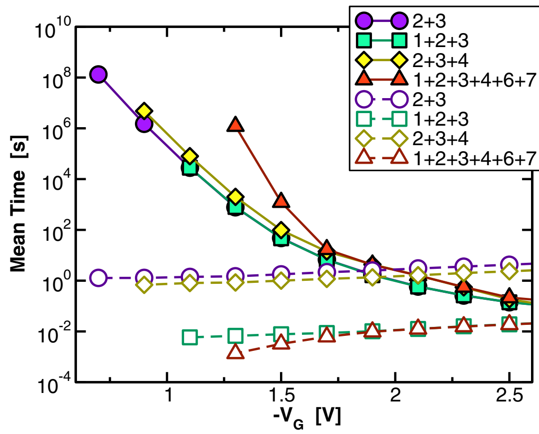

Fig. 9. Mean time to charge (filled symbols) for a certain number of defects at fixed bias V_G. Open symbols are the average dwelling times in this combined state.

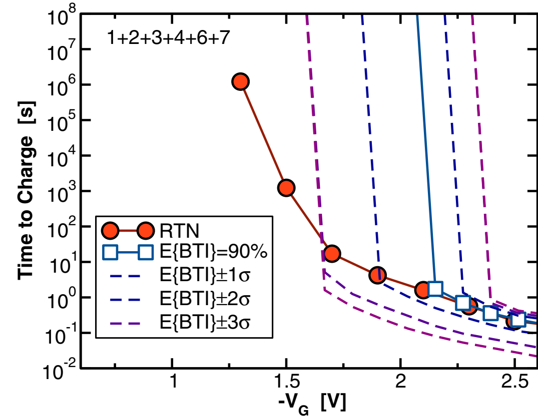

Fig. 10. Mean time to charge for all defects compared to the time it takes for these defects to become charged from the conventional NBTI perspective (expectation value of RTN). At low $|V_G|$, $\mathrm{E}\{\mathrm{BTI}\} \pm \sigma$ leads to wrong conclusions.

during conventional RTN analysis, they are very likely to occur sometime during long-term device operation.

Using the previously determined defect parameters, we can calculate the distribution of these events for a given defect subset. As an example, two realizations of such a stochastic process are shown in Fig. 7, considering only defects B1, B2, and B3 for demonstration. Also, once all defects have become charged, the dwelling time in this combined state will be dominated by the defect with the shortest emission time, in this case B1. The dwelling time is defined as the time were all defects remain in the charged state. The probabilities for this combined time-to-charge as well as the dwelling times for all identified defects are shown in Fig. 8, which are roughly exponential (note that the p.d.f.s are shown on a logarithmic time scale). For example, at $V_G = V_{DD} = -1.3\,\mathrm{V}$ it will take about 14 days on average for all defects to become charged at the same time, introducing a spontaneous $\Delta V_{th} \approx 20\,\mathrm{mV}$, considerably more than the ΔV_{th} caused by B1 and B3 (2 mV and 8 mV) individually. Given that our analysis only captures defects inside our measurement window, these 20 mV must be considered a lower bound.

The bias dependence of the mean time-to-charge as well as the mean dwelling time are shown in Fig. 9 for a few interesting combinations of defects. Clearly, while the mean time increases exponentially at lower $|V_G|$, these events are bound to occur during the lifetime of the device.

B. Consequences for Stochastic BTI

This observation must be contrasted to conventional NBTI analysis, which only considers the expectation value for this event [30]. As an example we consider a simple digital switch from a lower gate voltage V_G^L to a higher voltage V_G^H, not necessarily high enough to be considered 'stress'. For a device with given a set of defects with step heights $d_i = d_i(V_G^H)$, $\tau_{c,i}^H = \tau_{c,i}(V_G^H)$, $\tau_{e,i}^H = \tau_{e,i}(V_G^H)$, $\tau_{c,i}^L = \tau_{c,i}(V_G^L)$, and $\tau_{e,i}^L = \tau_{e,i}(V_G^L)$, the expectation value of the stochastic process leading to charge capture after a certain stress time t_s will be

$$\mathrm{E}\{\Delta V_{th}(t_s)\} = -\sum_i d_i a_i \left\{1 - \exp\left[-t_s\left(\frac{1}{\tau_{c,i}^H} + \frac{1}{\tau_{e,i}^H}\right)\right]\right\} \quad (2)$$

The factor a_i is the difference of the equilibrium occupancy probabilities and given by

$$a_i = \frac{\tau_{e,i}^H}{\tau_{e,i}^H + \tau_{e,i}^H} - \frac{\tau_{e,i}^L}{\tau_{e,i}^L + \tau_{e,i}^L}. \quad (3)$$

For large stress voltages and low initial voltages, a_i will be close to unity, meaning that the defect was almost certainly uncharged prior stress and almost certainly charged at the end of a stress phase much larger than the capture time. For lower high voltages, e.g. operating voltages, a_i may be smaller than unity for defects where $\tau_{c,i}^H \ll \tau_{e,i}^H$ is not fulfilled (in this case defect B3). For example, for $\tau_{c,i}^H \approx \tau_{e,i}^H$, the defect will only have a 50% chance of being occupied even after very long stress times, leading to additional variability in ΔV_{th}. Since during higher stress voltages this effect will be small, special care has to be taken not to miss this effect when extrapolating back to lower (and more relevant) use conditions. For example, as shown in Fig. 10, below a certain V_G the expectation value of the probability that all defects become charged never reaches the (arbitrary) threshold of 90% and the occurrence of this additional noise contribution is missed.

C. Statistical Relevance

In order to ensure that our observations on this single device are statistically relevant, we performed 1 ks RTN, 100 s NBTI stress, and 1 ks NBTI recovery plus RTN analysis on about 100 devices (at 25 °C and 125 °C, $V_s = -2.25\,\mathrm{V}$). In contrast to the previous analysis, only a single 1 ks recovery trace was available for every device, reducing the accuracy but considerably decreasing the duration of a single experiment. The complementary c.d.f. of the step-heights (pre-stress, NBTI recovery, post-stress) as well as the distribution of emission times is shown in Fig. 11. As expected, the distributions agree

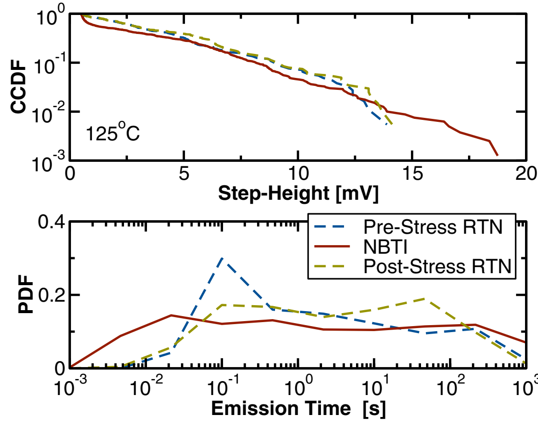

Fig. 11. RTN-NBTI-RTN experiments were performed on ≈100 nano-scale devices. For both RTN and NBTI, the step-height (top) as well as the emission time distributions (bottom) agree very well and are wider than the experimental window (1 ms – 1 ks for NBTI and 10 ms – 1 ks for RTN) and thus truncated.

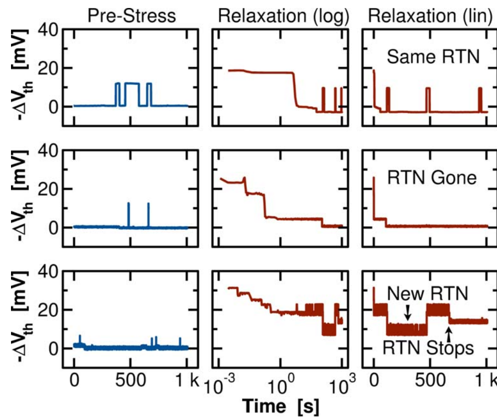

Fig. 12. Three typical cases of how NBTI interacts with the RTN signal: **Top**: RTN is unaffected by NBTI (100 s @ −2.25 V), which is the most likely scenario **Middle**: RTN disappears after NBTI, which occurs occasionally **Bottom**: New RTN is created by NBTI, which is the least likely case. Here, a case is shown where the newly created fast RTN disappears after 650 s, so this is possibly a temporary RTN signal as discussed previously [21].

very well, corroborating our findings that we are dealing with the same defects during RTN and BTI.

As a final piece of evidence that the responsible defects are the same we look at the recently observed volatility of BTI defects [18]. In these experiments it was found that the defects responsible for BTI can disappear and reappear on a wide range of time-scales, a finding recently confirmed by others [31]. Quite analogously, it has been observed a long time ago that RTN defects can disappear and reappear, a phenomenon termed anomalous RTN [32]. Also, it has been found that BTI stress can increase $1/f$ noise [19, 33], which, according to common perception, is the result of many superpositioned RTN defects. This increase of noise following BTI stress may partially be due to temporary RTN, which is caused by defects which produce RTN for a limited amount of time following a BTI stimulus [21]. We found this effect to be fully repeatable. Alternatively, it may happen that a truly new defect is created by BTI stress or a previously existing RTN defect is removed.

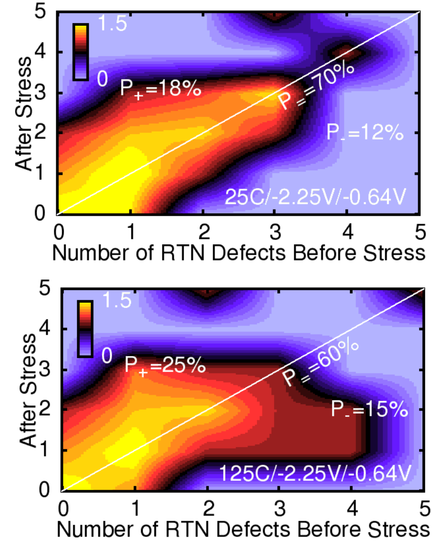

Fig. 13. The number of RTN defects fluctuates during operation. While most defects in this sample produced RTN both before and after NBTI stress (1 ks sampled at 20 ms), the number of RTN defects tends to increase on average after NBTI stress. Top is at 25 °C and bottom at 125 °C, which shows that at higher T the number of RTN defects increases somewhat more than at lower T (shown is $\log_{10}$(count)).

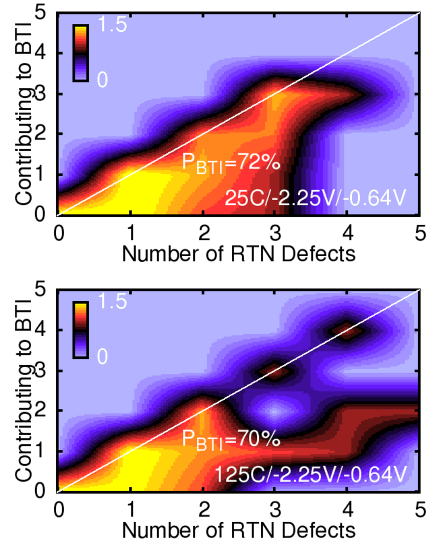

Fig. 14. Most defects contribute to both RTN and NBTI. About 70% of the defects that produced RTN in a 1 ks measurement sampled with 20 ms at $V_{\mathrm{th}} = -0.64$ V, also contribute to NBTI recovery within 1 ks after a 100 s stress at −2.25 V.

While the details behind all these processes are not yet fully understood, the essence is that both the number of defects producing RTN as well as the number of defects contributing to BTI recovery can change with time.

Three important cases are shown in Fig. 12: *(i)* RTN is unaffected by BTI stress, *(ii)* RTN has disappeared after BTI stress, and *(iii)* a new RTN defect is created following BTI. The probability for these cases to occur is studied in Fig. 13, which shows that RTN will predominantly be unaffected by BTI but that there is a 20% probability that the number of RTN defects increases. On average, the probability that defects

disappear is somewhat lower, consistent with the observation that NBTI in large-area devices tends to increase the noise level [19, 33]. Finally, Fig. 14 shows that about 70% of the defects that generate RTN also contribute a step to the BTI recovery trace. As for an RTN trap to contribute to BTI it is required that τ_c decreases with increasing $|V_G|$, which is not the case for all traps, particularly those closer to the gate contact [4, 34], this observation is perfectly consistent with the expectations.

IV. Conclusions

Based on multiple arguments and a detailed analysis at the single defect level, we conclude that RTN and the recoverable component of NBTI are due to the same defects. This implies that conventional RTN and BTI are only limiting cases of a much richer phenomenon and must therefore be characterized together for meaningful results. In particular, NBTI analysis enables the study of defects contributing to long-term RTN by decreasing the value of the capture time constant τ_c, thereby accelerating the charge capture process. These defects must also be considered from an RTN perspective, since they may become charged simultaneously by chance during the lifetime of the device, resulting in considerable but statistically occurring ΔV_{th} spikes, which may for instance lead to SRAM failures. Also, BTI around V_{DD} will have a large stochastic contribution not captured by standard models, making extrapolation from stress to operating conditions more challenging.

V. Acknowledgments

The research leading to these results has received funding from the FWF project n°23390-M24 and the European Community's FP7 project n°261868 (MORDRED)

References

[1] D. Fleetwood, ""Border Traps" in MOS Devices," *IEEE Trans.Nucl.Sci.*, vol. 39, no. 2, pp. 269–271, Apr 1992.

[2] D. Fleetwood, H. Xiong, Z.-Y. Lu, C. Nicklaw, J. Felix, R. Schrimpf, and S. Pantelides, "Unified Model of Hole Trapping, $1/f$ Noise, and Thermally Stimulated Current in MOS Devices," *IEEE Trans.Electron Devices*, vol. 49, no. 6, pp. 2674–2683, 2002.

[3] E. Simoen and C. Claeys, "Random Telegraph Signal: a Local Probe for Single Point Defect Studies in Solid-State Devices," *Mat.Sci.Eng.B*, vol. 91-92, pp. 136–143, 2002.

[4] T. Nagumo, K. Takeuchi, T. Hase, and Y. Hayashi, "Statistical Characterization of Trap Position, Energy, Amplitude and Time Constants by RTN Measurement of Multiple Individual Traps," in *Proc. Intl.Electron Devices Meeting (IEDM)*, 2010, pp. 628–631.

[5] V. Huard, M. Denais, and C. Parthasarathy, "NBTI Degradation: From Physical Mechanisms to Modelling," *Microelectronics Reliability*, vol. 46, no. 1, pp. 1–23, 2006.

[6] D. Ang, S. Wang, G. Du, and Y. Hu, "A Consistent Deep-Level Hole Trapping Model for Negative Bias Temperature Instability," *IEEE Trans.Dev.Mat.Rel.*, vol. 8, no. 1, pp. 22–34, 2008.

[7] B. Kaczer, T. Grasser, P. Roussel, J. Martin-Martinez, R. O'Connor, B. O'Sullivan, and G. Groeseneken, "Ubiquitous Relaxation in BTI Stressing – New Evaluation and Insights," in *Proc. Intl.Rel.Phys.Symp. (IRPS)*, 2008, pp. 20–27.

[8] T. Grasser, H. Reisinger, W. Goes, T. Aichinger, P. Hehenberger, P. Wagner, M. Nelhiebel, J. Franco, and B. Kaczer, "Switching Oxide Traps as the Missing Link between Negative Bias Temperature Instability and Random Telegraph Noise," in *Proc. Intl.Electron Devices Meeting (IEDM)*, 2009, pp. 729–732.

[9] B. Kaczer, T. Grasser, P. Roussel, J. Franco, R. Degraeve, L. Ragnarsson, E. Simoen, G. Groeseneken, and H. Reisinger, "Origin of NBTI Variability in Deeply Scaled PFETs," in *Proc. Intl.Rel.Phys.Symp. (IRPS)*, 2010, pp. 26–32.

[10] T. Wang, C.-T. Chan, C.-J. Tang, C.-W. Tsai, H. Wang, M.-H. Chi, and D. Tang, "A Novel Transient Characterization Technique to Investigate Trap Properties in HfSiON Gate Dielectric MOSFETs-From Single Electron Emission to PBTI Recovery Transient," *IEEE Trans.Electron Devices*, vol. 53, no. 5, pp. 1073–1079, 2006.

[11] C. Young, Y. Zhao, D. Heh, R. Choi, B. Lee, and G. Bersuker, "Pulsed Id-Vg Methodology and Its Application to Electron-Trapping Characterization and Defect Density Profiling," *IEEE Trans.Electron Devices*, vol. 56, no. 6, pp. 1322–1329, 2008.

[12] M. Toledano-Luque, B. Kaczer, J. Franco, P. Roussel, T. Grasser, T. Hoffmann, and G. Groeseneken, "From Mean Values to Distributions of BTI Lifetime of Deeply Scaled FETs Through Atomistic Understanding of the Degradation," in *IEEE Symposium on VLSI Technology Digest of Technical Papers*, 2011.

[13] M. Toledano-Luque, B. Kaczer, E. Simoen, P. J. Roussel, A. Veloso, T. Grasser, and G. Groeseneken, "Temperature and Voltage Dependences of the Capture and Emission Times of Individual Traps in High-k Dielectrics," *Microelectronic Engineering*, vol. 88, pp. 1243–1246, 2011.

[14] D. Veksler and G. Bersuker, "Gate Dielectric Degradation: Pre-Existing vs. Generated Defects," *J.Appl.Phys.*, vol. 115, no. 3, pp. 1–11, 2014.

[15] T. Grasser, T. Aichinger, G. Pobegen, H. Reisinger, P.-J. Wagner, J. Franco, M. Nelhiebel, and B. Kaczer, "The 'Permanent' Component of NBTI: Composition and Annealing," in *Proc. Intl.Rel.Phys.Symp. (IRPS)*, Apr. 2011, pp. 605–613.

[16] S. Mahapatra, K. Ahmed, D. Varghese, A. E. Islam, G. Gupta, L. Madhav, D. Saha, and M. A. Alam, "On the Physical Mechanism of NBTI in Silicon Oxynitride p-MOSFETs: Can Differences in Insulator Processing Conditions Resolve the Interface Trap Generation versus Hole Trapping Controversy?" in *Proc. Intl.Rel.Phys.Symp. (IRPS)*, 2007, pp. 1–9.

[17] S. Mahapatra, A. Islam, S. Deora, V. Maheta, K. Joshi, A. Jain, and M. Alam, "A Critical Re-evaluation of the Usefulness of R-D Framework in Predicting NBTI Stress and Recovery," in *Proc. Intl.Rel.Phys.Symp. (IRPS)*, 2011, pp. 614–623.

[18] T. Grasser, K. Rott, H. Reisinger, M. Waltl, P. Wagner, F. Schanovsky, W. Goes, G. Pobegen, and B. Kaczer, "Hydrogen-Related Volatile Defects as the Possible Cause for the Recoverable Component of NBTI," in *Proc. Intl.Electron Devices Meeting (IEDM)*, Dec. 2013.

[19] B. Kaczer, T. Grasser, J. Martin-Martinez, E. Simoen, M. Aoulaiche, P. Roussel, and G. Groeseneken, "NBTI from the Perspective of Defect States with Widely Distributed Time Scales," in *Proc. Intl.Rel.Phys.Symp. (IRPS)*, 2009, pp. 55–60.

[20] T. Grasser, K. Rott, H. Reisinger, P.-J. Wagner, W. Goes, F. Schanovsky, M. Waltl, M. Toledano-Luque, and B. Kaczer, "Advanced Characterization of Oxide Traps: The Dynamic Time-Dependent Defect Spectroscopy," in *Proc. Intl.Rel.Phys.Symp. (IRPS)*, Apr. 2013, pp. 2D.2.1–2D.2.7.

[21] T. Grasser, H. Reisinger, P.-J. Wagner, W. Goes, F. Schanovsky, and B. Kaczer, "The Time Dependent Defect Spectroscopy (TDDS) for the Characterization of the Bias Temperature Instability," in *Proc. Intl.Rel.Phys.Symp. (IRPS)*, May 2010, pp. 16–25.

[22] A. Asenov, R. Balasubramaniam, A. Brown, and J. Davies, "RTS Amplitudes in Decananometer MOSFETs: 3-D Simulation Study," *IEEE Trans.Electron Devices*, vol. 50, no. 3, pp. 839–845, 2003.

[23] J. Franco, B. Kaczer, M. Toledano-Luque, P. Roussel, J. Mitard, L. Ragnarsson, L. Witters, T. Chiarella, M. Togo, N. Horiguchi, G. Groeseneken, M. Bukhori, T. Grasser, and A. Asenov, "Impact of Single Charged Gate Oxide Defects on the Performance and Scaling of Nanoscaled FETs," in *Proc. Intl.Rel.Phys.Symp. (IRPS)*, 2012, p. 5A.4.1.

[24] M. Kirton and M. Uren, "Noise in Solid-State Microstructures: A New Perspective on Individual Defects, Interface States and Low-Frequency (1/f) Noise," *Adv.Phys.*, vol. 38, no. 4, pp. 367–486, 1989.

[25] G. Kapila and V. Reddy, "Impact of Sampling Rate on RTN Time Constant Extraction and its Implications on Bias Dependency and Trap Spectroscopy," *IEEE Trans.Dev.Mat.Rel.*, 2014, (in print).

[26] H. Reisinger, T. Grasser, and C. Schlünder, "A Study of NBTI by the Statistical Analysis of the Properties of Individual Defects in pMOSFETs," in *Proc. Intl.Integrated Reliability Workshop*, 2009, pp. 30–35.

[27] M. Waltl, P. Wagner, H. Reisinger, K. Rott, and T. Grasser, "Advanced Data Analysis Algorithms for the Time-Dependent Defect Spectroscopy of NBTI," in *Proc. Intl.Integrated Reliability Workshop*, 2012, pp. 74–79.

[28] H. Reisinger, “The Time-Dependent Defect Spectroscopy,” in *Bias Temperature Instability for Devices and Circuits*, T. Grasser, Ed. Springer, New York, 2014, pp. 75–110.

[29] D. Gillespie, “A General Method for Numerically Simulating the Stochastic Time Evolution of Coupled Chemical Reactions,” *J.Comp.Phys.*, vol. 22, pp. 403–434, 1976.

[30] M. Duan, J. Zhang, Z. Ji, W. Zhang, B. Kaczer, T. Schram, R. Ritzenthaler, G. Groeseneken, and A. Asenov, “New Analysis Method for Time-Dependent Device-To-Device Variation Accounting for Within-Device Fluctuation,” *IEEE Trans.Electron Devices*, vol. 60, no. 8, pp. 2505–2511, 2014.

[31] N. Tega, H. Miki, T. Mine, K. Ohmori, and K. Yamada, “Statistical Analysis of Relationship between Negative-Bias Temperature Instability and Random Telegraph Noise in Small p-channel Metal-Oxide-Semiconductor Field-Effect Transistors,” *Jap.J.Appl.Phys.*, vol. 53, pp. 1–6, 2014.

[32] M. Uren, M. Kirton, and S. Collins, “Anomalous Telegraph Noise in Small-Area Silicon Metal-Oxide-Semiconductor Field-Effect Transistors,” *Physical Review B*, vol. 37, no. 14, pp. 8346–8350, 1988.

[33] G. Kapila, N. Goyal, V. Maheta, C. Olsen, K. Ahmed, and S. Mahapatra, “A Comprehensive Study of Flicker Noise in Plasma Nitrided SiON p-MOSFETs: Process Dependence of Pre-Existing and NBTI Stress Generated Trap Distribution Profiles,” in *Proc. Intl.Electron Devices Meeting (IEDM)*, 2008, pp. 103–106.

[34] H. Miki, N. Tega, M. Yamaoka, D. J. Frank, A. Bansal, M. Kobayashi, K. Cheng, C. D’Emic, Z. Ren, S. Wu, J.-B. Yau, Y. Zhu, M. A. Guillorn, D.-G. Park, W. Haensch, E. Leobandung, and K. Torii, “Statistical Measurement of Random Telegraph Noise and Its Impact in Scaled-down High-κ/Metal-gate MOSFETs,” in *Proc. Intl.Electron Devices Meeting (IEDM)*, 2012, pp. 450–453.